Temperature effects on the crystallization kinetics of size-dependent systems in a continuous mixed-suspension mixed-product removal crystallizer

Jenn Fang Wu, Clifford Y. Tai, Wei Koun Yang, and Lii Ping Leu

Ind. Eng. Chem. Res., **1991**, 30 (9), 2226-2233 • DOI: 10.1021/ie00057a027

Temperature Effects on the Crystallization Kinetics of Size-Dependent Systems in a Continuous Mixed-Suspension Mixed-Product Removal Crystallizer

Jenn-Fang Wu, Clifford Y. Tai,* Wei-Koun Yang, and Lii-Ping Leu
Department of Chemical Engineering, National Taiwan University, Taipei, Taiwan 10764, R.O.C.

This study examined the nucleation and growth behaviors of potassium alum crystals in a well-mixed continuous crystallizer. Crystal growth rates are size dependent and surface integration controlled. The higher temperatures enhance the growth rate but depress the nucleation rate. The interface supersaturation, which is identical with the overall supersaturation in this study, decreases as the temperature is increased under the constraints of constant retention time and magma density. The predicted kinetic behaviors influenced by temperature were found to be in agreement with those of experimental results.

Introduction

The concept of a continuous mixed-suspension mixed-product removal (CMSMPR) crystallizer proposed by Randolph and Larson (1988) has become a useful and precise experimental technique for determining growth and nucleation rates. In a mixed-suspension crystallizer, the crystal size distribution is generally influenced by several factors including supersaturation, suspension density, agitation, temperature, and impurity concentrations. The effects of these factors in a well-mixed crystallizer have been reviewed by Garside and Shah (1980), Garside (1985), and Tavare (1986). However, relatively little work has been done to study and explain the effects of temperature on the crystallization kinetics in a CMSMPR crystallizer for size-dependent growth systems.

Genck and Larson (1972) studied the effects of temperature on nucleation (B°) and growth (G) rates of potassium nitrate and potassium chloride in a CMSMPR crystallizer. The temperature effects on the nucleation and growth rates under the constraints of constant suspension density and fixed retention time were apparently different and were dependent on the choice of solute. With potassium nitrate, G increased but B° decreased as the temperature was increased. On the other hand, G decreased but B° increased for potassium chloride. They explained their observations qualitatively by considering the effects of temperature on supersaturation and on the rate constants associated with nucleation and growth. However, the supersaturations were not reported in their study. Randolph and Cise (1972) used a transient CMSMPR crystallizer to study the crystallization kinetics of potassium sulfate. The nucleation and growth rates were calculated from the washout crystal size distribution measured by a multichannel high-speed automatic Coulter particle counter. They found that the nucleation and growth rates increased as the temperature was increased, but the results were limited to crystal size range (1.3–26.0) $\times 10^{-6}$ m. With utilization of the same apparatus operated at quasi-steady state, the crystallization kinetics of magnesium sulfate and citric acid were studied, and the supersaturation was measured by using a Bausch and Lomb Abbe 3L refractometer (Sikdar and Randolph, 1976). They found that the nucleation rates of both systems decreased. However, the growth rate of citric acid increased and that of magnesium sulfate was only slightly influenced as the temperature was increased for crystal size in the range (4.5–70.0) $\times 10^{-6}$ m.

With an attempt to find the crystallization kinetics of potassium nitrate, Helt and Larson (1977) measured the concentrations of solutions using a differential refractometer. Owing to the low level of supersaturation exhibited by potassium nitrate in a CMSMPR crystallizer, their results are somewhat scattering and inconclusive. They observed G increased and B° decreased as the temperature was increased at constant supersaturation and suspension density; i.e., the activation energy of growth was positive but that of nucleation was negative for potassium nitrate. Rousseau and Woo (1980) studied the effects of temperature and impurity on the nucleation and growth rates of potassium alum crystals in a CMSMPR crystallizer. The authors used the Abegg–Stevens–Larson (ASL) model to express the size-dependent growth rate and developed an Arrhenius type equation to correlate nucleation and growth rates with crystallization temperature. They found that the temperature had a stronger influence on nucleation rate than growth rate at nearly constant suspension density, agitation rate, and supersaturation level. However, the supersaturations of potassium alum solutions in the crystallizer were not measured. A mathematical analysis was carried out by Wey and Terwilliger (1980) to examine the effects of temperature on the nucleation and growth rates in CMSMPR crystallizers. Their study provided a reasonable basis to understanding the kinetic behaviors of nucleation and growth rates. Under the constraints of constant suspension density and fixed retention time in a CMSMPR crystallizer, variations in the nucleation and growth rates with temperature could be predicted from the respective activation energy and the relative kinetic order between nucleation and growth. The analysis was illustrated by a size-independent system. Qian et al. (1987) studied the crystallization kinetics of potassium chloride from brine in a CMSMPR crystallizer. They found that the growth rate increased but the nucleation rate decreased as the temperature was increased. Again, supersaturation was not reported in their study. In the above, the systems studied were size-independent for crystal growth rates except that by Rousseau and Woo (1980).

In this study, we considered the size-dependent growth rate of potassium alum crystals and developed a detailed analysis of temperature effects on the nucleation and growth rates in a CMSMPR crystallizer. The concentration of potassium alum solution was measured by using a density meter, and the nucleation and growth rates were obtained from the crystal size distributions at steady-state conditions. Under the constraints of constant suspension density and retention time, the predicted kinetic behaviors influenced by temperature were compared with those of experimental results.

Population Balance and Crystallization Kinetics

When a CMSMPR crystallizer is operated at steady state with no crystal breakage and no crystals in the feed

0888-5885/91/2630-2226$02.50/0

stream, the number balance on the crystals in this crystallizer leads to the equation

$$\frac{d(Gn)}{dL} = -\frac{n}{\tau} \quad (1)$$

Assuming the crystal growth rates follow the ASL model (Abegg et al., 1968)

$$G = G^\circ(1 + \gamma L)^b; \quad b < 1 \quad (2)$$

The parameter γ in (2) is often set equal to $1/G^\circ\tau$ in order to reduce the complexity. Substituting (2) into (1) and solving the resulting differential equation gives crystal size distribution as

$$n = n^\circ\left(1 + \frac{L}{G^\circ\tau}\right)^{-b} \exp\left[\frac{1 - (1 + L/G^\circ\tau)^{1-b}}{1 - b}\right] \quad (3)$$

The suspension density M_T was integrated to give (O'Dell and Rousseau, 1978)

$$M_T = C_1(b)\rho k_v n^\circ (G^\circ\tau)^4 \quad (4)$$

where $C_1(b)$ was correlated with b by Rousseau and Parks (1981) as shown by

$$C_1(b) = \exp[1.79 + 4.27b - 14.97b^2 + 71.96b^3 - 121.25b^4 + 79.05b^5] \quad (5)$$

Substitute (4) into (3) to eliminate n°:

$$n = \frac{M_T}{C_1(b)\rho k_v (G^\circ\tau)^4}\left[1 + \frac{L}{G^\circ\tau}\right]^{-b} \times \exp\left[\frac{1 - (1 + L/G^\circ\tau)^{1-b}}{1 - b}\right] \quad (6)$$

Using (6) to fit the population density data, G° and b can be evaluated. This method (Rousseau and Parks, 1981) is similar to that used by Jancic and Garside (1976) except without extrapolating the population density data to find n°. Therefore, the values of G° and b converge more quickly by using the random search method or other search methods.

The nucleation rate B° is related to the nuclei growth rate, G°, and nuclei population density, n°, by the following equation:

$$B^\circ = n^\circ G^\circ \quad (7)$$

On the basis of the two-step model, the growth rate can be expressed as the following equations:

$$G = K_D \exp(-E_D/RT)(\sigma - \sigma_i) \quad \text{mass-transfer step}$$

$$= K_r \exp(-E_r/RT)\sigma_i^{n_r} \quad \text{surface-integration step} \quad (8a)$$

at $L = 0$

$$G^\circ = K_D^\circ \exp(-E_D^\circ/RT)(\sigma - \sigma_i^\circ)$$

$$= K_r^\circ \exp(-E_r^\circ/RT)\sigma_i^{\circ n_r^\circ} \quad (8b)$$

where σ_i and σ_i° are the interfacial supersaturations for crystal sizes L and 0, respectively.

Since secondary nuclei are generated from the crystal surface or solid/solution interface, part of them survive to form small crystals in the bulk solution (Bauer et al., 1974). Consider that the number of nuclei generated is a function of interfacial supersaturation and the portion of nuclei survived is a function of overall supersaturation (Tai et al., 1991). It is reasonable to express the nucleation rate in terms of interfacial supersaturation, overall supersaturation, suspension density, and temperature by the following form:

$$B^\circ = K_B \exp(-E_B/RT)\sigma^{n_{B1}}\sigma_i^{n_{B2}}M_T^j \quad (9)$$

Table I. Effects of Increased Temperature on G and B° at Constant σ and M_T for CMSMPR Crystallizers Operated at Conditions of Negligible Mass-Transfer Resistance [Judged from (10a), (10b), and (11)]

	$E_B > 0$	$E_B > 0$
$E_r > 0$	$G\uparrow B^\circ\uparrow$	$G\uparrow B^\circ\downarrow$
$E_r < 0$	$G\downarrow B^\circ\uparrow$	$G\downarrow B^\circ\downarrow$

Table II. Effects of Increased Temperature on G°, B°, and σ at Constant τ and M_T for CMSMPR Crystallizers Operated at Conditions of Negligible Mass-Transfer Resistance [Judged from (12), (13), and (14)]

	$E_B - iE_r^\circ > 0$	$E_B - iE_r^\circ < 0$
$E_B + 3E_r^\circ > 0$	$G^\circ\downarrow B^\circ\uparrow \sigma\downarrow$	$G^\circ\uparrow B^\circ\downarrow \sigma\downarrow$
$E_B + 3E_r^\circ < 0$	$G^\circ\downarrow B^\circ\uparrow \sigma\uparrow$	$G^\circ\uparrow B^\circ\downarrow \sigma\uparrow$

If the mass-transfer resistance of crystal growth is negligible in stirred crystallizers, the value of σ_i will approach that of σ. Thus (8a), (8b), and (9) can be simplified as follows.

$$G = K_r \exp(-E_r/RT)\sigma^{n_r} \quad (10a)$$

$$G^\circ = K_r^\circ \exp(-E_r^\circ/RT)\sigma^{n_r^\circ} \quad (L = 0) \quad (10b)$$

$$B^\circ = K_B \exp(-E_B/RT)\sigma^{n_B}M_T^j \quad (11)$$

where $n_B = n_{B1} + n_{B2}$.

For pure systems operated at constant hydrodynamic conditions, K_B and K_r (K_r°) can be regarded as constants. Substitution of (7), (10b), and (11) into (4) gives an expression for supersaturation:

$$\sigma = \left\{\frac{\exp[(E_B + 3E_r^\circ)/RT]}{C_1(b)\rho k_v K_B (K_r^\circ)^3 \tau^4 M_T^{j-1}}\right\}^{1/[n_r^\circ(i+3)]} \quad (12)$$

where $i = n_B/n_r^\circ$. Substituting (12) into (10b) and (11), we obtain the following equations for nuclei growth rate and nucleation rate without measuring the supersaturation in a CMSMPR crystallizer.

$$G^\circ = \left[\frac{(K_r^\circ)^i}{C_1(b)\rho k_v K_B}\right]^{1/(i+3)} \times \exp\left[\frac{E_B - iE_r^\circ}{(i+3)RT}\right] M_T^{(1-j)/(i+3)}\tau^{-4/(i+3)} \quad (13)$$

$$B^\circ = \left[\frac{K_B^3}{C_1(b)^i \rho^i k_v^i (K_r^\circ)^{3i}}\right]^{1/(i+3)} \times \exp\left[\frac{-3(E_B - iE_r^\circ)}{(i+3)RT}\right] M_T^{(i+3j)/(i+3)}\tau^{-4i/(i+3)} \quad (14)$$

From (13) and (14), it can be seen that temperature would influence the growth and nucleation rates in an opposite way under constant σ and M_T. The slope of the plot of $\ln B^\circ$ versus $1/T$ and that of the plot of $\ln G^\circ$ versus $1/T$ will differ by a factor of -3. The effects of increased temperature on supersaturation, nucleation rate, and growth rate will depend on the values of E_B, E_r, E_r°, and i as summarized in Tables I and II for constant σ, M_T and constant τ, M_T, respectively.

Experiment Apparatus and Procedure

A schematic flow diagram of this experiment is shown in Figure 1. The apparatus is a cooling, continuous, mixed-suspension, mixed-product removal crystallizer which was used to crystallize potassium alum from aqueous solution. The crystallizer shown in Figure 2 is a cylindrical acrylic vessel equipped for four baffles. Its active volume

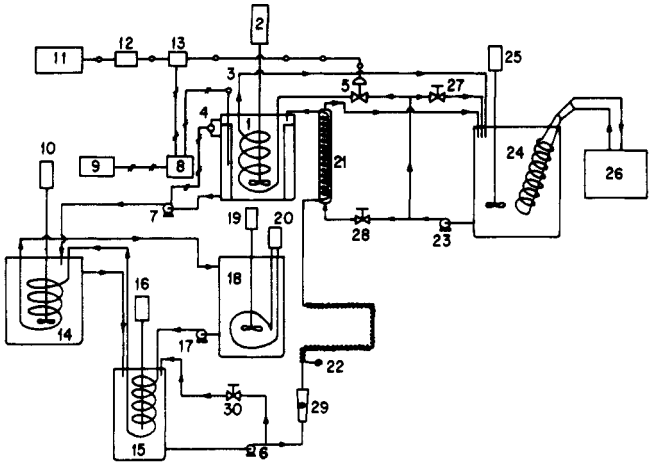

Figure 1. Flow diagram of CMSMPR crystallizer: 1, crystallizer; 2, variable-speed stirrer; 3, thermocouple; 4, liquid level controller; 5, control valve; 6, feed pump; 7, withdrawal pump; 8, temperature controller; 9, temperature recorder; 10, stirrer; 11, air compressor; 12, air regulator; 13, I/P converter; 14, feed tank 1; 15, feed tank 2; 16, stirrer; 17, hot water pump; 18, hot water tank; 19, stirrer; 20, heater; 21, precooler; 22, heating tape; 23, cooling water pump; 24, cooling water tank; 25, stirrer; 26, refrigerator; 27, global valve; 28, global valve; 29, flowmeter; 30, needle valve.

was held constant at 5.7×10^{-3} m^3 and was agitated by a four-blade 45° pitch turbine located 48×10^{-3} m from the bottom of the crystallizer. A partial draft tube was formed by a tightly wound coil of 316 stainless steel tube. The stirrer pumped the solution downward inside the draft tube.

The feed solution was held in two dissolving tanks in series with a capacity of 38×10^{-3} m^3 (tank 1) and 26×10^{-3} m^3 (tank 2), respectively. The temperatures of these two tanks were kept at 10 K higher than the saturation temperature of the solution by supplying heat through a wound coil in which the hot water was flowing. The solution was pumped by a FMI piston pump through a rotameter, a heated glass tube, and a precooler and then entered the crystallizer. The heated glass tube was used to dissolve small crystals that might be carried over from the dissolver; the precooler was used to cool the solution to a temperature that was just 2–3 K higher than the set point of the crystallizer and thus to minimize temperature fluctuation in the crystallizer. No crystals were detected by eye or by the Microtrac particle size analyzer before the feed solution entered the crystallizer. The flow rate and concentration (C_{in}) of feed solution were determined by a precalibrated flowmeter and density meter. When they were stable, the experiment was started. About 30 min later, the temperature of the crystallizer was able to keep within ±0.05 K of the set point by a temperature control system consisting of a temperature controller (Leeds & Northrup), an air regulator, an I/P converter, a cooling coil, a control valve, and a refrigerated water bath.

The impeller speed was controlled at 700 rpm in all experimental runs. The product withdrawal port was located at the same height as the impeller. The purpose of this arrangement was to ensure isokinetic removal of the well-mixed suspension. The magma was removed from the crystallizer with a self-priming slurry pump (ITT-JABSCO) activated intermittently by an electronic liquid level controller (COLE-PARMER). Approximately 250×10^{-6} m^3 of suspension was removed during each pumping cycle; thus the level of the solution in the crystallizer was kept essentially constant in all runs.

In each run, two magma samples, 400–500 mL for each sample, were withdrawn from the crystallizer through the

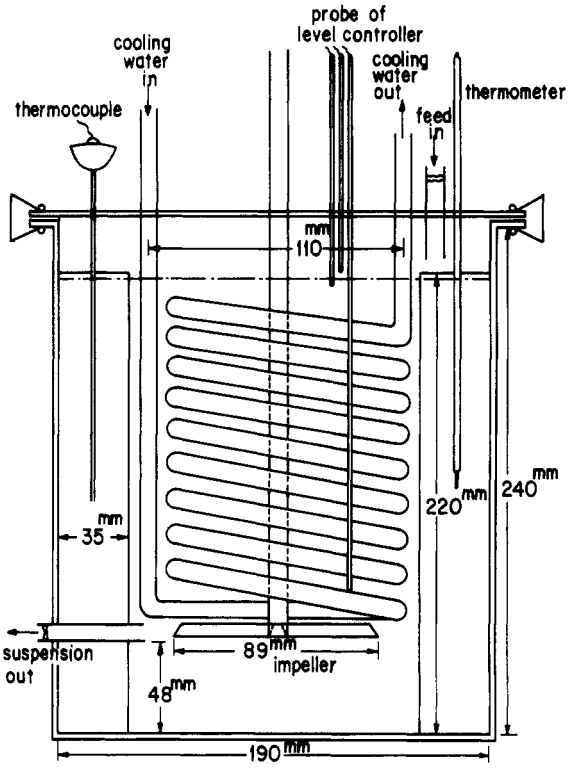

Figure 2. Configuration of crystallizer.

product withdrawal port. One was taken at between 10τ and 12τ and the other between 15τ and 17τ. The magma samples were filtered rapidly. Then the cakes (crystals) were washed by a small amount of deionized water and acetone and then dried by air. The crystal size distributions of these two crystal samples were determined by sieve analysis for the size range $(251–1245) \times 10^{-6}$ m and by a L & N Microtrac particle size analyzer for the size range $(2–251) \times 10^{-6}$ m. The filtrates were heated to dissolve the nuclei that were possibly formed during filtration, and the concentrations C of the filtrates were determined by a density meter (Kyoto Electronics DA-210). Then the supersaturation σ was calculated as $(C - C_{sat})/C_{sat}$. The accuracy of the density meter was $\pm 2 \times 10^{-5}$ g/cm^3, which was approximately equivalent to ±0.02 K of supersaturated temperature for the potassium alum–water system. We calibrated the density meter by using deionized water and dry air before the solution density was measured. The density measuring cell was kept at 303.15 ± 0.02 K by circulating constant-temperature water outside the cell. When the density was measured, measuring time about 2–3 min, the concentration of the solution could be evaluated by using the predetermined density–concentration correlations or the plots of density vs concentration. Essentially there was no difference for crystal size distribution and filtrate concentration between the samples taken at the two retention times; thus the steady state was achieved after 10τ.

The weight W of the crystal sample was checked with the concentrations of feed solution and filtrate by the following equations:

$$W_1 = V_1 \rho_1 \frac{C_{in} - C}{1 + C} \tag{15}$$

$$\text{percent difference} = \left| \frac{W - W_1}{W_1} \right| \times 100\% \tag{16}$$

The percent difference was always smaller than 10% for all runs. It ensured that a steady state and an isokinetic

Table III. Values of System and Model Parameters for Various Residence Times and Different Temperatures

run no.	T, K	σ	$10^8G°$, m/s	$10^{-7}B°$, no./(m³·m)	M_T(from (15)), kg/m³	M_T(expt), kg/m³	τ, s	b
1	298	0.0802	2.83	0.973	19.4	19.0	1240	0.443
2	298	0.0669	1.16	2.325	21.3	20.9	1520	0.582
3	298	0.0618	1.37	0.936	22.3	22.5	2110	0.480
4	298	0.0750	1.94	3.008	21.1	22.2	1140	0.511
5	298	0.0831	2.10	2.878	16.3	15.0	940	0.537
7	298	0.0838	2.54	6.014	13.9	15.8	770	0.475
8	293	0.0772	1.54	4.121	30.0	28.6	1260	0.541
12	293	0.0746	1.31	4.177	23.3	22.6	1250	0.576
14	293	0.0763	1.38	2.956	16.6	15.0	1240	0.550
15	293	0.0947	3.05	1.158	12.1	11.6	1010	0.428
17	288	0.0954	1.51	4.051	35.8	33.0	1330	0.542
19	288	0.0839	1.10	2.866	36.8	34.2	2180	0.457
20	288	0.0975	0.95	5.141	28.3	28.6	1660	0.556
22	293	0.0833	2.88	9.331	31.2	29.8	770	0.446
23	293	0.0597	0.69	2.307	34.2	34.3	2780	0.543
25	293	0.0974	2.51	2.712	33.9	32.1	630	0.485
26	293	0.0579	0.74	2.427	28.0	28.0	2670	0.503
27	288	0.1321	2.27	26.65	33.2	33.5	630	0.534
29	288	0.1237	1.48	27.52	28.0	29.7	730	0.591
30	288	0.0639	0.49	1.892	31.6	31.1	3680	0.544
31	288	0.0876	0.86	18.34	26.0	26.7	1170	0.595
33	283	0.0986	0.77	29.34	29.3	30.8	1070	0.628
34	283	0.1234	0.90	60.79	25.9	27.0	740	0.640
35	283	0.0949	0.77	16.97	25.0	26.3	1200	0.622
37	283	0.0825	0.58	5.53	19.6	19.3	2040	0.580
39	283	0.0750	0.38	4.94	16.4	16.1	2360	0.634
40	283	0.0700	0.26	5.67	16.9	17.5	2970	0.644
42	283	0.0936	0.64	10.02	25.0	24.6	1670	0.593

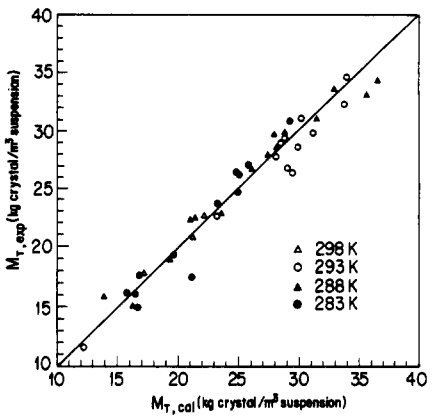

Figure 3. Comparison of experimental suspension density with calculated suspension density from (15).

removal of suspension had been achieved. The crystallization temperatures conducted in this experiment were 283, 288, 293, and 298 K. The volumetric flow rates of the feed solution were between 1.55×10^{-6} and 9.15×10^{-6} m³/s.

Result and Discussion

Forty-two runs were performed in which potassium alum was crystallized from aqueous solution using the equipment and procedures described in the previous section. Suspension densities calculated by (15) and obtained by experiment are shown in Figure 3. The agreement between these two values is excellent. Besides that the achievement of steady state and isokinetic removal of suspension should be ensured, the concentration or supersaturation of potassium alum solution could be measured accurately by using a density meter. The supersaturated temperatures are from 1.2 to 3.4 °C for 42 runs summarized in Table III. In a CMSMPR crystallizer the supersaturation of solution was often declared to be very low and unmeasurable in previous papers. For potassium alum–water system the supersaturation of solution had been measured in this study and in the literature (Jancic and Garside, 1976). The crystals were very easily grown to 1000×10^{-6} m or larger in 10τ. Except in systems with a very narrow metastable region, the supersaturation of solution in a CMSMPR crystallizer should be measurable. Otherwise, the growth rate of crystal would be very small so that the crystals were grown with difficulty to 1000×10^{-6} m or larger.

The population densities were calculated from crystal mass distributions (Randolph and Larson, 1988) by a sieve analysis [for a crystal size range $(251–1245) \times 10^{-6}$ m] and a Microtrac particle size analyzer [for a crystal size range $(2–251) \times 10^{-6}$ m]. From population density data, a nonlinear least-squares parameter estimation program, random search method, was used to estimate b and $G°$ in (6) by minimizing the objective function

$$F = \sum_{i=1}^{k} [\ln n_i(\text{expt}) - \ln n_i(\text{calc})]^2 \qquad (17)$$

The initial value of b was set between 0 and 0.99 and that of $G°$ between 10^{-7} and 10^{-9} m/s. The searching range contracted by a factor of 0.55 per cycle. The point with minimum objective function value in 130 points was taken as the middle point for the next searching cycle. Twenty-four searching cycles were used in our program so that the last searching ranges were smaller than 10^{-3} and 10^{-10} m/s for b and $G°$, respectively. The maximum error should be less than 1% in the evaluation of b and $G°$. Further increasing in searching points and searching cycles did not improve our results. As shown in Figure 4, by example, the fit to the data is good. The population density curves obtained in our experiment look similar to those presented by Rousseau and Woo (1980), that is, curvature exhibited over the entire size range. Values of system variables and model parameters are summarized in Table III. The values of b determined in this experiment are between 0.40 and 0.65, which increase slightly as the temperature decreases. The values are somewhat different from those reported by Rousseau and Woo (1980), between 0.60 and 0.70, and by Jancic and Garside (1976),

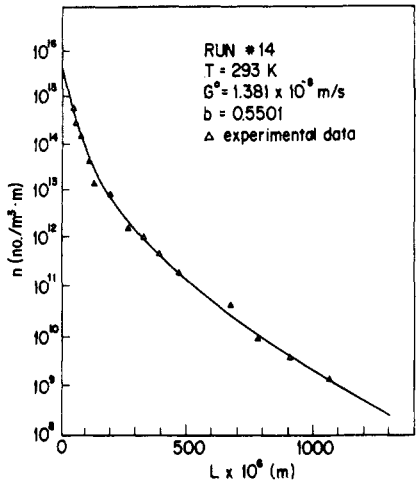

Figure 4. Plot of crystal size distribution for run 14.

Table IV. Comparison of Estimating Methods for Nucleation Rate and Growth Rate Proposed by Jones et al. (1986) and Rousseau and Parks (1981)

run no.	$10^{-7}B°$	$10^8G°$	10^8G (4 μm)	10^8G (20 μm)	10^8G (50 μm)	10^8G (200 μm)
Method Proposed by Jones et al. (1986)						
3	1.0	0.70	1.2	1.7	2.3	3.7
10	5.9	1.4	2.0	2.6	3.2	4.7
14	3.3	0.65	1.3	2.1	3.0	5.6
20	4.7	0.57	1.1	1.7	2.3	4.0
32	3.1	0.45	0.47	0.76	1.0	2.0
38	7.9	0.73	0.73	1.3	1.9	3.9
Method Proposed by Rousseau and Parks (1981)						
3	0.94	1.4	1.5	1.7	2.2	3.7
10	6.0	1.9	2.0	2.4	3.0	4.7
14	3.0	1.4	1.5	2.1	2.9	5.6
20	5.1	0.95	1.1	1.5	2.1	4.0
32	3.1	0.45	0.51	0.72	1.0	2.0
38	8.1	0.62	0.76	1.2	1.8	3.9

between 0.55 and 0.75. The possible reason for the discrepancy was due to the lower bound of crystal size used in the data analysis, because the experimental data of the population density were much scattered at smaller crystal sizes. In this study the lower bound of crystal size used in the data analysis is 27×10^{-6} m.

In the determination of growth and nucleation rates, the results are sensitive to the curvature of population density plot, especially in the small-size range. Jones et al. (1986) used an empirical equation, (18), to fit population density data.

$$\ln n = P_1 \exp(P_2 L^{0.5} + P_3 L) \tag{18}$$

They calculated growth rate from (19) (Sikdar, 1977)

$$G(L) = \frac{N(L)}{n(L)\tau} \tag{19}$$

Owing to the abnormally increase in the population density of small-size crystals, the integration of $n(L)$ to obtain $N(L)$ will give a large error. The comparison of results obtained by the method used in this study (Rousseau and Parks, 1981) and that by Jones et al. (1986) is listed in Table IV. The calculated growth and nucleation rates give good agreement between these two methods, except the growth rates of crystal approaching zero size. The larger discrepancy for zero size was due to extrapolation uncertainty.

The ASL size-dependent growth rate model used in this study gives good fit to population density data as shown in Figure 4. That the growth rate of potassium alum is size-dependent has been verified by Garside and Jancic (1976) and Tai et al. (1990). Certainly, the growth rate dispersion model, which fits population density data as well as the ASL model, can be used to explain the population density curve that deviates from a straight line. From the viewpoint of screw dislocation theory, the size-dependent growth rate and growth rate dispersion are possible.

Table V. The Parameters in (8a) and (9) for Five Different Crystal Sizes

10^6L	K_D	E_D	K_r	E_r	K_B[a]	E_B[b]
0	c	c	2.1×10^8	78389	6.7×10^{-1}	−46834
20	c	c	9.5×10^4	58663	7.0×10^2	−36256
50	c	c	4.9×10^3	50692	6.7×10^3	−32627
200	c	c	1.4×10^2	40564	4.6×10^4	−29295
1000	c	c	6.4×10^0	31098	6.2×10^4	−28296

[a] Calculated from the values of K_B/K_r^i and i listed in Table VI. [b] Calculated from the values of $iE_r - E_B$ and i listed in Table VI. [c] The results were not converged by random search method.

If the crystal growth can be expressed by the two-step model, i.e., (8a), we may eliminate σ_i and set $n_r = 2$ (Tai and Lin, 1987) to give

$$\sigma G^{-1/2} = \bar{K}_D^{-1} G^{1/2} + \bar{K}_r^{-1/2} \tag{20}$$

where

$$\bar{K}_r = K_r \exp(-E_r/RT)$$

$$\bar{K}_D = K_D \exp(-E_D/RT)$$

The slope and the intercept of the plot, $\sigma G^{-1/2}$ versus $G^{1/2}$, would be used to calculate the values of $\bar{K}_D$ and $\bar{K}_r$, respectively. The slopes obtained in this study are very close to zero; thus the value of $\bar{K}_D$ is either a very large number or a negative number for every temperature and every crystal size. It means that the mass-transfer resistance was negligible. An alternative way to evaluate mass-transfer and surface-integration coefficients is by setting an objective function F_1

$$F_1 = \sum_{i=1}^{42} \{G^{1/2}[K_D \exp(-E_D/RT)]^{-1} - \sigma G^{-1/2} + [K_r \exp(-E_r/RT)]^{-1/2}\}_i^2 \tag{21}$$

where i represents the ith run. A random search method was used to evaluate K_D, E_D, K_r, and E_r by minimizing the objective function F_1. The values of K_r and E_r converged and are listed in Table V, but those of K_D and E_D did not converge after a long searching time for every crystal size. Therefore, it can be concluded that the mass-transfer resistance of crystal growth is negligible and the interface supersaturation σ_i is identical with the overall supersaturation σ for potassium alum crystals when they are crystallized from a stirred-tank crystallizer operated at 700 rpm.

In CMSMPR crystallizers the solution sustains a slightly lower level and narrower range of supersaturation (σ = 0.0579–0.1321 in this study), which becomes less at larger retention time. In the study of crystallization kinetics the supersaturation must be measured accurately. To avoid the measurement of supersaturation, one can substitute (10a) into (11) to give (22) by eliminating σ:

$$B° = \frac{K_B}{K_r^i} G^i M_T^j \exp[(iE_r - E_B)/RT] \tag{22}$$

where $i = n_B/n_r$. The values of K_B/K_r^i, i, j, and $iE_r - E_B$ were evaluated by linear regression for different crystal sizes and are listed in Table VI. The order j of suspension density is close to 1 for every crystal size. The magma densities conducted in this experiment are between 11 and 36 kg/m^3. A crystallizer operated at such magma density

Table VI. The Parameters in (22) for Seven Different Crystal Sizes

10^6L	K_B/K_r^i	i	j	$iE_r - E_B$
0	3.8×10^{-8}	0.871	1.002	115 107
20	9.3×10^{-5}	1.381	0.989	117 267
50	1.3×10^{-2}	1.546	1.010	111 008
100	4.8×10^{-1}	1.634	1.033	104 657
200	1.1×10^{1}	1.689	1.061	97 799
500	3.2×10^{2}	1.718	1.102	88 550
1000	2.5×10^{3}	1.714	1.135	81 598

is considered to be a lean one. The first order on magma density is consistent with the results of Ottens and de Jong (1973) that the crystal–wall and crystal–impeller collisions should be the major mechanisms of nucleation.

The relative kinetic order i of nucleation to growth is about 1.5 except the one of zero size. The growth rate of zero size is calculated by extrapolating the population density data, so it will give a larger error. From the values of relative kinetic order i we know that the nucleation rate depends on the supersaturation more strongly than the growth rate does. Therefore, the crystallizer should be kept at a lower level of supersaturation to produce larger crystals. Because the mass-transfer resistance is negligible when compared to the surface-integration resistance for crystal growth, the overall supersaturation order of growth rate will approach interfacial supersaturation order n_r of the surface-integration rate. The value of n_r has been confirmed to be 2 for potassium alum crystals (Tai et al., 1990). When (10a) was used directly to correlate experimental data, the values of n_r were 1.62, 1.78, 1.82, 1.86, and 1.87, for crystal sizes 0, 20×10^{-6}, 50×10^{-6}, 200×10^{-6}, and 1000×10^{-6} m, respectively, not just 2. Notwithstanding this, the values of n_r confined to be 2 should be appropriate.

The values of E_B were calculated from the values of $iE_r - E_B$, i, and E_r and are listed in Table V. The nucleation rate decreases as the temperature is increased. The values of the mass-transfer coefficients are very large and the mass-transfer resistance is negligible when compared to surface integration resistance. Therefore, the correct values of the mass-transfer coefficients are not obtainable in a stirred-tank crystallizer for the potassium alum–water system. The activation energy E_r of the surface integration rate is 3.1×10^4 to 7.8×10^4 J/mol for crystal size range from 0 to 1000×10^{-6} m. The values of E_r obtained in this study are compared to 4.3×10^4 J/mol obtained by Garside and Mullin (1968) and 5.0×10^4 J/mol by Budz et al. (1985) and are of the same order as heat of solution and heat of fusion.

A survey of the temperature effect on crystal growth and nucleation rates is summarized in Table VII. In most cases an increase in growth rate is accompanied by a decrease in nucleation rate when the temperature is increased. In early work Genck and Larson (1972) did not measure the supersaturation in the crystallizer. The observed kinetic behavior was a combined result of temperature and supersaturation effects. There are still two cases, Randolph and Cise (1972) and Rousseau and Woo (1980), in contradiction to others. Although the mechanisms of the temperature effect on nucleation and crystal growth are not clear, it is possible that the cluster on the crystal surface is more active and thus the surface-integration rate is faster at higher temperature. Therefore, the growth rate should be faster at higher temperature. When the cluster incorporates into the crystal, partial water molecules drain away to disintegrate other clusters on a nearby crystal surface into smaller clusters. At higher temperatures the growth rate is faster, so the equilibrium

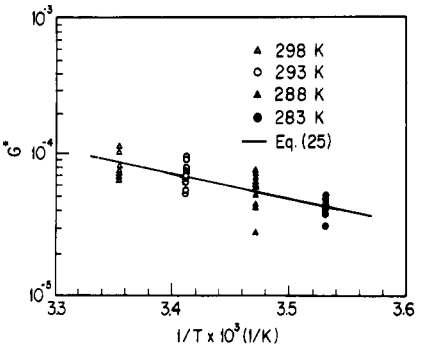

Figure 5. Plot of G^* versus $1/T$.

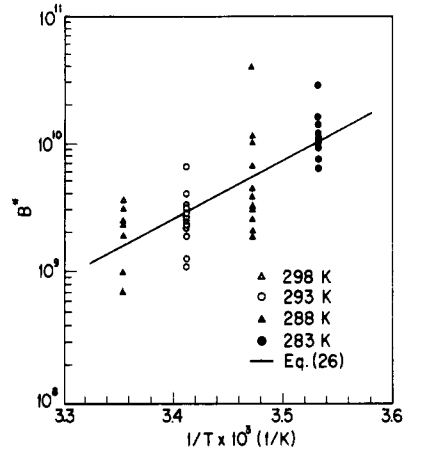

Figure 6. Plot of B^* versus $1/T$.

mean size of clusters is smaller. Also, the smaller clusters gather to nucleate with more difficulty. Therefore, the secondary nucleation rate decreases as the temperature is increased. Certainly, the processes of nucleation and growth are very complex. The mechanisms of the temperature effect will not be resolved until the mechanisms of secondary nucleation are clear.

It is extremely difficult to keep both M_T and τ constant while changing the crystallization temperature. Besides, the value of b, and thus that of $C_1(b)$, varies from run to run as shown in Table III. To illustrate the temperature effect on nucleation and nuclei growth rate under the constraints of constant M_T and τ, we define G^* and B^* by rearranging (13) and (14):

$$G^* = G^\circ C_1(b)^{1/(i+3)} M_T^{(j-1)/(i+3)} \tau^{4/(i+3)}$$

$$= \left[\frac{(K_r^\circ)^i}{\rho k_v K_B}\right]^{1/(i+3)} \exp[(E_B - iE_r^\circ)/[(i+3)RT]] \quad (23)$$

$$B^* = B^\circ C_1(b)^{i/(i+3)} M_T^{-(i+3j)/(i+3)} \tau^{4i/(i+3)}$$

$$= \left[\frac{K_B^3}{\rho^i k_v^i (K_r^\circ)^{3i}}\right]^{1/(i+3)} \exp[-3(E_B - iE_r^\circ)/[(i+3)RT]] \quad (24)$$

Once the parameters in (10b) and (11) are determined, as listed in Tables V and VI, G^* and B^* can be predicted as a function of temperature.

$$G^* = 14.16 \exp(-3576/T) \quad (25)$$

$$B^* = 3.80 \times 10^{-7} \exp(10730/T) \quad (26)$$

Equations 25 and 26 are plotted in Figures 5 and 6. Data points, calculated by (23) and (24) using experimental

Table VII. Survey of Temperature Effect on Crystal Growth and Nucleation Rates

system	response to increasing temp	crystallizer type and oper mode	equip. used to measure supersaturation	reference
potassium chloride	$G\downarrow$ $B^\circ\uparrow$	CMSMPR steady state	*a*	Genck and Larson (1972)
potassium nitrate	$G\uparrow$ $B^\circ\downarrow$	CMSMPR steady state	*a*	Genck and Larson (1972)
potassium sulfate	$G\uparrow$ $B^\circ\uparrow$	CMSMPR transient	*a*	Randolph and Cise (1972)
citric acid	$G\uparrow$ $B^\circ\downarrow$	CMSMPR quasi steady state	refractometer	Sikdar and Randolph (1976)
magnesium sulfate	$G?$ $B^\circ\downarrow$	CMSMPR quasi steady state	refractometer	Sikdar and Randolph (1976)
potassium nitrate	$G\uparrow$ $B^\circ\downarrow$	CMSMPR steady state	differential refractometer	Helt and Larson (1977)
potassium alum	$G\uparrow$ $B^\circ\uparrow$	CMSMPR steady state	*b*	Rousseau and Woo (1980)
potassium alum	$G\uparrow$ $B^\circ\downarrow$	fluidized bed	*c*	Budz et al. (1985)
potassium chloride	$G\uparrow$ $B^\circ\downarrow$	CMSMPR steady state	*a*	Qian et al. (1987)
potassium alum	$G\uparrow$ $B^\circ\downarrow$	CMSMPR steady state	density meter	this study

[a] Supersaturation was not reported. [b] Level of supersaturation was not reported but was kept constant along with suspension density and agitation rate. [c] Equipment used to measure supersaturation was not illustrated.

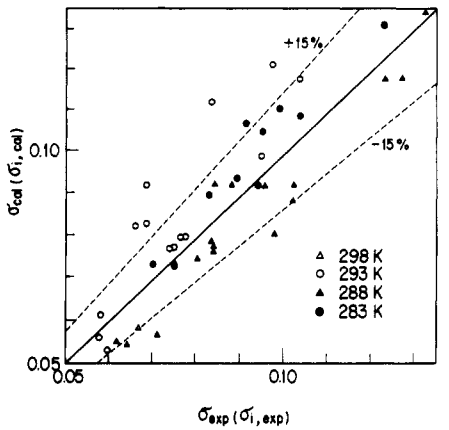

Figure 7. Comparison of experimental supersaturation with calculated supersaturation from (12).

values G°, B°, $C_1(b)$, M_T, τ, i, and j, are also shown in the figures. Although the data points are rather scattered, the arithmetic mean of each temperature level is fairly close to that predicted by (25) and (26). Under the constraints of constant M_T and τ, i.e., constant production rates, the nucleation and growth rates always vary with temperature in opposite directions.

Since the value of $(E_B + 3E_r^\circ)$ is positive, the supersaturation of potassium alum solution in the crystallizer operated at constant M_T and τ is lowered as the temperature is increased. The interfacial supersaturation is equal to overall supersaturation, because the mass-transfer resistance of crystal growth is negligible. Figure 7 shows the consistancy of supersaturation between the values calculated from (12) and those measured experimentally in this study. Most of the data points are within ±15% of the calculated values.

Conclusion

The ASL model was found to be suitable for the size-dependent growth rate of potassium alum crystals. On the basis of the two-step model, the mass-transfer resistance is negligible for crystal growth in our stirred-tank crystallizer. Thus the interfacial supersaturation is equal to supersaturation of bulk solution. The effects of supersaturation on the nucleation rate are stronger than those on the growth rate. The nucleation rate is chiefly attributed to crystal–wall and crystal–impeller collisions in consideration of the first-order dependence on magma density.

The higher temperature enhances the growth rate but depresses the nucleation rate slightly. The activation energy of surface integration rate is about 5.5×10^4 J/mol; that is of the same order as heat of solution or heat of fusion and is in agreement with the results reported in the literature. Under the constraints of constant retention time and magma density, the nucleation rate decreases quickly and the growth rate increases slightly as the temperature is increased.

Acknowledgment

We gratefully acknowledge the support of the National Science Council of the Republic of China through Grant NSC 75-0402-E002-09.

Nomenclature

b = kinetic parameter in ASL growth rate equation
B° = nucleation rate, number/(m^3·s)
B^* = nucleation rate function defined in (24)
C = solution concentration in crystallizer, kg of hydrate/kg of H_2O
C_i = solution concentration at crystal/solution interface, kg of hydrate/kg of H_2O
C_{in} = feed solution concentration, kg of hydrate/kg of H_2O
$C_1(b)$ = moment coefficient defined in (5) for two-parameter ASL model
C_{sat} = solution concentration at saturation, kg of hydrate/kg of H_2O
E_B = activation energy of nucleation rate, J/mol
E_D = activation energy of mass-transfer rate, J/mol
E_D° = activation energy of mass-transfer rate for zero-size crystals, J/mol
E_r = activation energy of surface integration rate, J/mol
E_r° = activation energy of surface integration rate for zero-size crystals, J/mol
F = objective function defined in (17)
F_1 = objective function defined in (21)
G = crystal growth rate, m/s
G° = nuclei growth rate, m/s
G^* = growth rate function defined in (23)
$i = n_B/n_r$, relative kinetic order
j = kinetic order of suspension density in nucleation rate model
k_v = volumetric shape factor
K_B = nucleation rate constant in (9)

K_D = mass-transfer coefficient in two-step model, m/s
$K_D°$ = mass-transfer coefficient for zero-size crystals, m/s
$\bar{K}_D$ = mass-transfer coefficient in (20), m/s
K_r = surface-integration coefficient in two-step model, m/s
$K_r°$ = surface-integration coefficient for zero-size crystals, m/s
$\bar{K}_r$ = surface-integration coefficient in (20), m/s
L = equivalent diameter or crystal size, m
L_i = equivalent diameter or crystal size, m
M_T = suspension density, kg/m^3
n = population density, number/(m^3·m)
n_i = population density at crystal size L_i, number/(m^3·m)
$n°$ = population density of zero-size crystals, number/(m^3·m)
n_B = kinetic order of supersaturation in nucleation rate model, (11)
n_{B1} = kinetic order of supersaturation in nucleation rate model, (9)
n_{B2} = kinetic order of interfacial supersaturation in nucleation rate model, (9)
n_r = kinetic order of interfacial supersaturation in surface integration rate model, (8a)
$n_r°$ = kinetic order of interfacial supersaturation in surface integration rate model for zero-size crystals, (8b)
$N(L)$ = cumulative number oversize, number/m^3
P_1, P_2, P_3 = parameters in (18)
R = gas constant, J/(mol·K)
T = temperature, K
V_1 = sampled solution volume, m^3
W = sampled crystal weight, kg
W_1 = calculated crystal weight from (15), kg

Greek Letters

γ = parameter in the ASL growth rate equation
ρ = crystal density, kg/m^3
ρ_1 = solution density, kg/m^3
τ = retention time, s
$\sigma = (C - C_{sat})/C_{sat}$, relative supersaturation
$\sigma_i = (C_i - C_{sat})/C_{sat}$, interfacial supersaturation
$\sigma_i°$ = interfacial supersaturation of nuclei

Literature Cited

Abegg, C. F.; Stevens, J. F.; Larson, M. A. Crystal Size Distribution in Continuous Crystallizers When Growth Rate Is Size Dependent. *AIChE J.* **1968**, *14*, 118–122.

Bauer, L. G.; Rousseau, R. W.; McCabe, W. L. Influence of Crystal Size on the Rate of Contact Nucleation in Stirred-Tank Crystallizers. *AIChE J.* **1974**, *20*, 653–659.

Budz, J.; Karpinski, P. H.; Nuruc, Z. Effect of Temperature on Crystallization and Dissolution Processes in a Fluidized Bed. *AIChE J.* **1985**, *31*, 259–268.

Garside, J. Industrial Crystallization from Solution. *Chem. Eng. Sci.* **1985**, *40*, 3–26.

Garside, J.; Jancic, S. J. Growth and Dissolution of Potash Alum Crystals in the Subsieve Size Range. *AIChE J.* **1976**, *22*, 887–894.

Garside, J.; Mullin, J. W. The Crystallization of Aluminium Potassium Sulphate: A Study in the Assessment of Crystallizer Design Data. III: Growth and Dissolution Rates. *Trans. Inst. Chem. Eng.* **1968**, *46*, T11–T18.

Garside, J.; Shah, M. B. Crystallization Kinetics from CMSMPR Crystallizers. *Ind. Eng. Chem. Process Des. Dev.* **1980**, *19*, 509–514.

Genck, W. J.; Larson, M. A. Temperature Effects of Growth and Nucleation Rates in a Mixed Suspension Crystallization. *AIChE Symp. Ser.* **1972**, *68* (No. 121), 57–66.

Helt, J. E.; Larson, M. A. Effects of Temperature on the Crystallization of Potassium Nitrate by Direct Measurement of Supersaturation. *AIChE J.* **1977**, *23*, 822–830.

Jancic, S. J.; Garside, J. A New Technique for Accurate Crystal Size Distribution Analysis in a MSMPR Crystallizer. In *Industrial Crystallization*; Mullin, J. W., Ed.; Plenum: New York, 1976; pp 363–372.

Jones, A. G.; Budz, J.; Mullin, J. W. Crystallization Kinetics of Potassium Sulfate in a MSMPR Agitated Vessel. *AIChE J.* **1986**, *32*, 2002–2009.

O'Dell, F. P.; Rousseau, R. W. Magma Density and Dominant Size for Size Dependent Crystal Growth. *AIChE J.* **1978**, *24*, 738–741.

Ottens, E. P. K.; de Jong, E. J. A Model for Secondary Nucleation in a Stirred Vessel Cooling Crystallizer. *Ind. Eng. Chem. Fundam.* **1973**, *12*, 179–184.

Qian, R. Y.; Chen, Z. D.; Ni, H. G.; Fan, Z. Z.; Cai, F. D. Crystallization Kinetics of Potassium Chloride from Brine and Scale-up Criterion. *AIChE J.* **1987**, *33*, 1690–1697.

Randolph, A. D.; Cise, M. D. Nucleation Kinetics of the Potassium Sulfate-Water System. *AIChE J.* **1972**, *18*, 798–807.

Randolph, A. D.; Larson, M. A. *Theory of Particulate Processes*; Academic Press: New York, 1988.

Rousseau, R. W.; Woo, R. Effects of Operating Variables on Potassium Alum Crystal Size Distribution. *AIChE Symp. Ser.* **1980**, *76* (No. 193), 27–33.

Rousseau, R. W.; Parks, R. M. Size-dependent Growth of Magnesium Sulfate Heptahydrate. *Ind. Eng. Chem. Fundam.* **1981**, *20*, 71–76.

Sikdar, S. K. Size-dependent Growth Rate from Curved Log n(L) vs. L Steady State Data. *Ind. Eng. Chem. Fundam.* **1977**, *16*, 390–398.

Sikdar, S. K.; Randolph, A. D. Secondary Nucleation in a Mixed Suspension Crystallizer: Magnesium Sulfate and Citric Acid Water Systems. *AIChE J.* **1976**, *22*, 110–117.

Tai, C. Y.; Lin, C. H. Crystal Growth Kinetics of Two-step Model. *J. Cryst. Growth* **1987**, *82*, 377–384.

Tai, C. Y.; Wu, J. F.; Shih, C. Y. Crystal Growth Mechanism of Size-dependent Systems in a Fluidized Bed. *J. Chem. Eng. Jpn.* **1990**, *23*, 562–567.

Tai, C. Y.; Wu, J. F.; Rousseau, R. W. Interfacial Supersaturation, Secondary Nucleation, and Crystal Growth. Submitted for publication in *J. Cryst. Growth* **1991**.

Tavare, N. S. Mixing in Continuous Crystallizers. *AIChE J.* **1986**, *32*, 705–732.

Wey, J. S.; Terwilliger, J. P. Effects of Temperature on Suspension Crystallization Processes. *Chem. Eng. Commun.* **1980**, *4*, 297–305.

Received for review April 9, 1991
Accepted May 15, 1991